Engineered Science
DOI: https://dx.doi.org/10.30919/es8d806

Metallic State and Negative Permittivity in $LaCo_{1-x}Ni_xO_3$ Ceramics

Zaixin Wei,[1] Gongyu Zhang,[1] Xiaoting Song,[1] Yingjie Wang,[1] Hengtong Wang,[1] Muqi Gao,[1] Huanrong Tian,[1] Wenjun Cai,[1] Yao Liu,[1,*] Zhongyang Wang,[2,*] Zidong Zhang[1,*] and Runhua Fan[3]

Abstract

The development of epsilon-negative materials are essential for many applications in smart electronics and modern information technology because of their enticing properties. Numberous efforts have been done in terms of diluted metal. However, no more attempt has been made from increasing electron density. And the effect of doping on negative permittivity is still unclear. In this work, mono-phase $LaCo_{1-x}Ni_xO_3$ (x =0.06, 0.1, 0.12, 0.16, 0.2) were prepared through a sol-gel technique and subsequent sintering. Electronic structure, electrical properties and negative permittivity properties are investigated in detail, and the correlation between electrical conductivity and negative permittivity is elaborated in terms of electrodynamics.

Keywords: Negative permittivity, LaCo1-xNixO3 ceramics, Electrical conducitivity.
Received: 27 September 2022; Revised: 23 November 2022; Accepted: 23 January 2023.
Article type: Research article.

1. Introduction

Epsilon-negative materials (ENMs), as a branch of metamaterials, have been promising candidates to be used in smart electronics and modern information technology.[1,2] Consequently, over the past ten years, interest in ENMs has persisted, and most efforts have been made to develop ENMs, and to incorporate ENMs in devices for various applications, such as high-power microwave filters,[3] coil-free electrical inductors,[4] novel capacitors,[5] electromagnetic shielding.[6] Though at first glance a permittivity equal to a negative value might seem exotic, naturally occurring materials do exhibit negative permittivity response below plasma frequency (typically in the UV band). Therefore, almost all metals can be regarded as ENMs. However, at radio-frequency, their complex permittivities are essentially missing due to the strong electric-field screening effect and large electron density, which leaves them little room to extern their capabilities. One classic strategy is to dilute the effective concentration of electrons. Typically, Pendry *et al.* pioneered periodic structures composed of very thin metal wires to dilute the average concentration of electrons and significantly increased the effective electron mass through self-inductance, and realized negative permittivity at GHz band.[7] Fan *et al.* extended and developed this strategy into natural materials.[8-12] They theoretically and experimentally investigated radio-frequency negative permittivity based on percolative composites, owing to the accessibility of construction of conducting path or percolative network through well-designed metal nano-fillers in the ceramic matrix and the complexity manipulated by changing the loading and morphology of fillers, such as dimensions, shapes and chemical surface modification process. The electron density of metal nanoparticle in the composite is diluted by the matrix with respect to bulk metal, therefore, from the viewpoint, composite can be seen as diluted metal.[13-16] Following the design principle for negative permittivity properties in composites, Guo *et al.* realized metacomposites with weakly negative permittivity response through the combination of polymer and carbon materials, such as carbon nanotubes,[17,18]

[1] *Key Laboratory for Liquid-Solid Structural Evolution and Processing of Materials (Ministry of Education), Shandong University, Jinan 250061, China.*
[2] *State Key Lab of Metal Matrix Composites, School of Materials Science and Engineering, Shanghai Jiao Tong University, Shanghai 200240, China.*
[3] *College of Ocean Science and Engineering, Shanghai Maritime University, Shanghai 201306, China.*
**Email:* liuyao@sdu.edu.cn (Y. Liu); zy_wang@sjtu.edu.cn (Z. Wang); zhangzidong@sdu.edu.cn (Z. Zhang)

carbon nanofibers[19,20] and graphene[21] because of their moderate electron density.

In addition to the diluted metal, currently, there are has been increased interest to achieve negative permittivity in terms of increasing electron concentration. Degenerately doped semiconductors, such as indium-tin-oxide (ITO) and aluminum-doped zinc oxide (AZO), may all feature a negative permittivity at radio-frequency band because they are both transparent and conductive.[22,23] Their dispersion can be regulated as a function of carrier dopant concentration, sintering atmospheres, or post-deposition annealing. Another typical configuration is through insulator-metal transition, mainly in the perovskite structure. Upadhyay *et al.* observed change in the conduction mechanism at a critical transition temperature in Sn-doped Sr_2MnO_4 ceramics and achieved negative permittivity.[24] They attributed the behavior to plasma oscillations of thermally excited free charge carriers and analyzed it using the Drude-Lorentz model. Similarly, Yan *et al.* attained negative permittivity in Sn-doped $LaMnO_3$ ceramics due to plasma oscillation of delocalized electrons from Mn 3d-electrons, and the dielectric dispersion can be controlled by Sr-dopants amounts.[25] The ability of perovskite oxides of cobalt to achieve an insulator-metal transition through dynamically modulating spin state configurations provides a natural and feasible platform for developing radio-frequency negative permittivity response. In addition, the inorganic perovskite defects induced by doping can significantly enhance the polarizability. Numerous studies have demonstrated that the Sr^{2+} partially substituted La^{3+} can provide change in spin state of Co^{3+} from low spin state to high spin state and improve the charge transport performance.[26,27] Furthermore, it was found that after partial replacement La^{3+} site with Ba^{2+} in $LaCoO_3$, part of Co^{3+} would be converted to Co^{4+}, bringing about high electrical conductivity and consequently realized negative permittivity.[28] Although B-site doping, such as Ni doping, has been extensively studied for excellent electrical properties, it is unclear that effect of doping on negative permittivity in $LaCoO_3$ system. Here, $LaCo_{1-x}Ni_xO_3$ (x =0.06, 0.1, 0.12, 0.16, 0.2) with perovskite structures were synthesized through a sol-gel technique. And their electrical properties and negative pemittivity properties were investaged in detail.

2. Experimental section

2.1 Preparation of $LaCo_{1-x}Ni_xO_3$ ceramics

$LaCo_{1-x}Ni_xO_3$ (x =0.06, 0.1, 0.12, 0.16, 0.2) ceramics were prepared via a sol-gel technique and sintering process. The pre-set molar ratio of $La(NO_3)_3 \cdot 6H_2O$ (Sigma-Aldrich, purity ≥ 99.0%), $Co(NO_3)_2 \cdot 6H_2O$ (Sigma-Aldrich, purity ≥ 99.0%) and $Ni(NO_3)_2 \cdot 6H_2O$ (Sigma-Aldrich, purity ≥ 99.0%) dissolved deionized water with magnetic stirring, citric acid monohydrate (Sinopharm Chemical Reagent Co. Ltd., purity≥99.5%) as the chelating agent. After vigorous blending, the mixture solution was heated under 80 °C while kept stirring moderately until the start of gelation. Subsequently, the obtained gel was treated at the temperature of 200 °C to remove residual water and citric acid monohydrate. Calcination was then carried out under 800°C for 2h to facilitate Ni doping into $LaCoO_3$ lattices and stabilize the crystal structure. Finally, the calcined powders were compacted in a model after grinding, forming green body with a size of ϕ20 mm × 2 mm. The resulting bodies were sintered with pressureless at 1200°C for 4h under an air atmosphere.

2.2 Characterization

Phase compositions were identified using X-ray diffraction (XRD, D/Max2550VB, Japan) and X-ray photoelectron spectroscopy (XPS, Axis Supra, UK). Microstructures and morphology were recorded using a thermal field scanning electron microscope (TF-SEM, SU-70, Japan). For the dielectric measurements, silver paste was sputtered on both sides of the sample disks. One side was entirely sputtered with the silver paste, while the other side was sputtered using an annular shadow mask with internal and external diameters of 6.4 mm and 10 mm, respectively. The RF permittivity and impedance were measured using an LCR meter (Keysight E4980AL, USA) equipped with a 16451B dielectric test fixture. Open and short compensations were performed before dielectric property testing.

3. Results and discussion

3.1 Composition and morphology

The SEM images in Fig. 1 illustrate designed specimens that feature relatively compact microstructures and grains with clear rhombus surfaces. A great number of boundaries exist among grains, no matter how much Ni is introduced, which is beneficial to weaken phonon scatter without affecting electron transport. Moreover, the average size of grain is reduced, revealing that the introduction of Ni can inhibit grain growth.

Figure 2(a) shows XRD patterns of all specimens, according to the JCPDF file number 48-0123 card, demonstrating slightly distorted perovskite structures with rhombohedral phases. Measured diffraction peaks corresponding to the planes (110 and 104) for all samples show an overall shift with initially moving toward lower angle and then to reset. Since the ionic radius of Ni^{2+} (0.68 Å) is larger than that of Co^{3+} (0.63 Å), the substitution of Co by Ni causes the deformation of octahedron. In terms of Bragg's equation ($2d\sin\theta=n\lambda$), diffraction peak shifting towards a

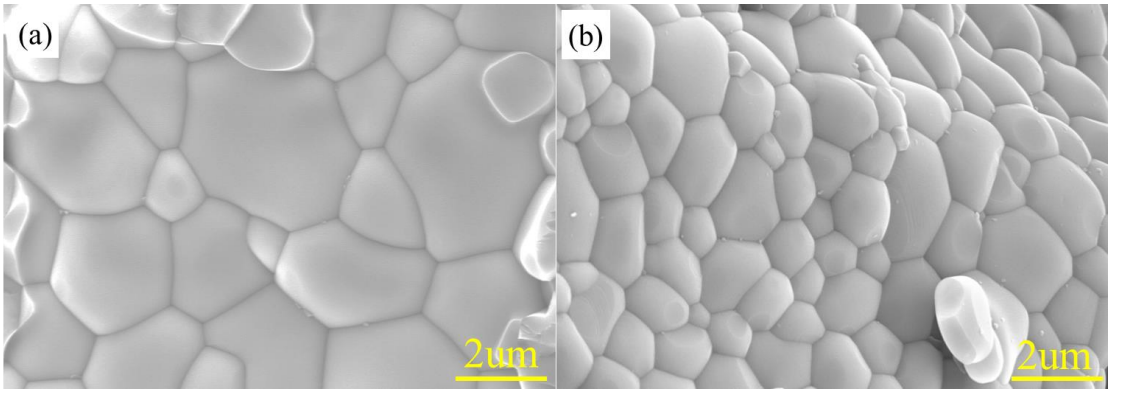

Fig. 1 SEM images of $LaCo_{1-x}Ni_xO_3$ ceramics: (a) $LaCo_{0.84}Ni_{0.06}O_3$ and (b) $LaCo_{0.8}Ni_{0.2}O_3$.

lower angle is due to the progressively larger interplanar spacing.[29] Furthermore, with the increase in Ba contents, the unimodal diffraction peaks at around 33.3° transform to bimodal ones, showing that the crystal structure of perovskite is distorted. Those also demonstrate that Co atoms are successfully replaced by Ni atoms.

To gain an in-depth understanding of the evolution mechanism of electrical and dielectric properties in $LaCo_{1-x}Ni_xO_3$, the deconvolution of Co 2p and O 1s were carried out based on XPS results. As depicted in Figs. 3(a, b, c), Co 2p spectra were split into two peaks of Co $2p_{3/2}$ and Co $2p_{1/2}$, corresponding with lower binding energy of nearly 780.2 eV and higher binding energy of around 795.7 eV, respectively.[30] The fitting results for the two distinguished characteristic peaks indicate Co are present as a mixture of Co^{2+} and Co^{3+} in the products. The Co^{3+} ion in the $LaCo_{1-x}Ni_xO_3$ system predominates, while a small amount of Co^{2+} ions are trapped probably because of $Co(NO_3)_2$. With increasing Ni content, Co^{3+} tends to increase, and Co^{2+} content undergo a variation with first increasing and then sharply decline (Fig. 3(d)). On the other hand, the substitution of Co by Ni was accompanied by the changes in oxygen vacancies and lattice oxygen. The O 1s spectra were split into three peaks representing the lattice oxygen (O_I), absorbed oxygen (O_{II}) and surface adsorbed water (O_{III}), respectively. The O_{II} mainly contains oxygen molecules and oxygen atoms captured by oxygen vacancies.[31] In terms of defect reactions, the generation of oxygen vacancies can be expressed, e.g. $La^{3+}Co_{\delta}^{3+}Co_{0.9-\delta}^{2+}Ni_{0.1}^{2+}O_3^{2-} + (1-\delta)/O_o^x, O_o^x \rightarrow 1/2O_2(g) + V_{\ddot{o}} + 2e^-$, here $\delta \ll 1$ and $V_{\ddot{o}}$ represents oxygen vacancies with two charges that would emerge as O atoms escaped from the crystal lattice. As shown in Fig. 4(d), the content of lattice oxygen reduces with increasing Ni-doping amounts to keep electrical neutrality.

3.2 Electrical properties and negative permittivity properties

Figure 5 shows the electrical conductivity spectra of $LaCo_{1-x}Ni_xO_3$ ceramics at room temperature. It can be seen that electrical conductivity strongly depends on the Ni-substituting amounts, while its dependence of frequency is weaker. As

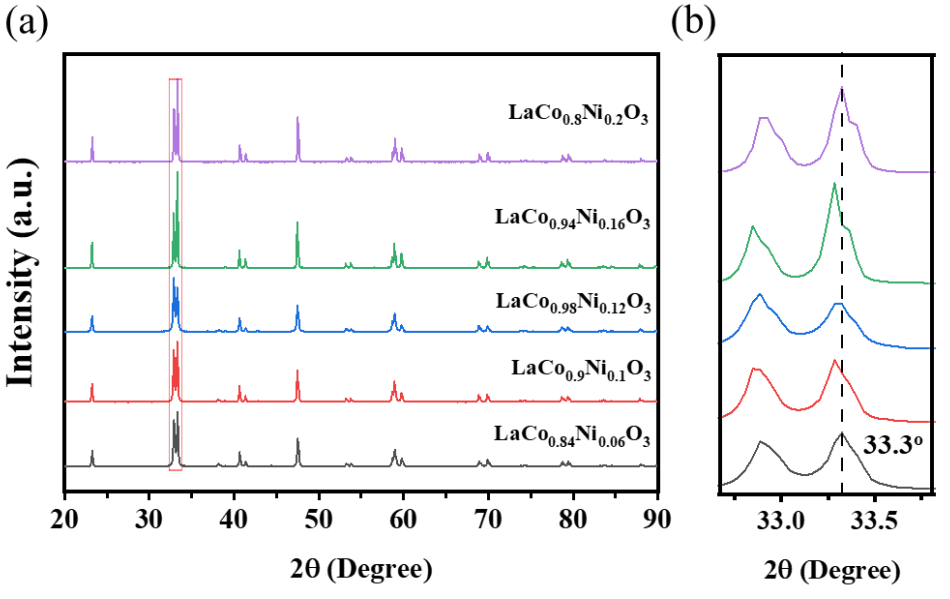

Fig. 2 XRD patterns of the $LaCo_{1-x}Ni_xO_3$ ceramics with different Ni contents (a) and the corresponding enlarge image (b).

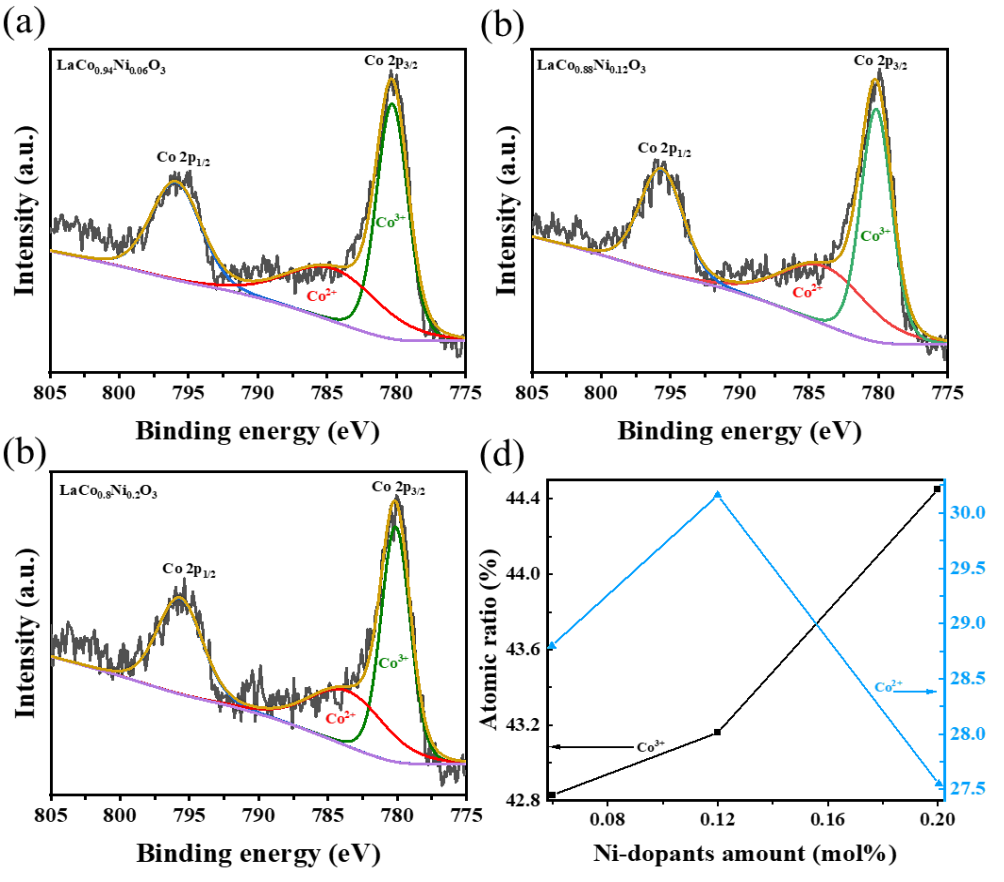

Fig. 3 High-resolution spectra of Co 2p (a-c) and atomic ratio of Co^{3+} and Co^{2+} (d).

mentioned above, the incorporation of Ni in $LaCo_{1-x}Ni_xO_3$ ceramics generates divalent oxygen vacancies that can act as donor impurities, inducing additional weakly bonding electrons. Under the external electric field, the electrons change from the local state to the itinerant state, like free electrons in a metal. On the other hand, the incorporation of Ni leads to the deformation of octahedron and change in Co^{3+} and Co^{2+} content. Those favor the transition of Co^{3+} from low spin (S=0) to intermediate-spin (S=1) or high-spin (S=2) state, which would enhance electrical conductivity. As shown in Fig. 5(a), the electrical conductivity of specimen with $x = 0.12$ reaches up to 0.16 $s.cm^{-1}$ at 100 kHz. It is a relatively large value in comparison to data previously reported.[32] In addition, all designed specimens show Drude response, though skin effect is less pronounced in higher frequencies. The phenomenon can be approximatively described by following Eq. (1).[33,34]

$$\sigma_{ac} = \frac{\sigma_{dc}\omega_\tau^2}{\omega^2+\omega_\tau^2} \quad (1)$$

Where σ_{dc} denotes dc limit for Drude model, ω_τ is the damping parameter. The fitted results are nearly identical with the experimental data. Transport properties studies on $LaCo_{1-x}Ni_xO_3$ demonstrated that speciman can be regarded as a metal-like in terms of electrical conductivity's dependence on frequency. It is found that σ_{ac} is not monotonous with Ni-doping amount, and the curve of $\sigma_{ac} - x$ is like a distorted and inverted V-shape (Fig. 5(b)). That implies that σ_{ac} exhibits an upper limit, and its maximum value would appear when x is between 0.12 and 0.14. Such an analogous variation in perovskite structure also reported by Delorme *et al*, and they attributed it to mutative oxygen vacancy.[35]

Radio-frequency negative permittivity properties of $LaCo_{1-x}Ni_xO_3$ ceramics are shown in Fig. 6. In the current testing band, permittivity of all specimens are negative value and exhibit the Drude response, in agreement with their electrical properties (Fig. 6(b)). Under an external electrical field, extensive electrons will collectively oscillate, inducing a plasmonic state. In presence of fact that it is at radio-frequency, it can be regarded as a low-frequency plasmonic state. According to Drude model, the permittivity is described as follows.[36,37]

$$\varepsilon' = 1 - \frac{\omega_p^2}{\omega^2+\omega_\tau^2} \quad (2)$$

where $\omega_p = \sqrt{\frac{ne^2}{m^*\varepsilon_0}}$ denotes plasma frequency, with n being the electron density, m^* being the effective electron mass, ε_0 being the vacuum permittivity, and e being the electron charge. The fact that Eq. (2) is well matched to experiment data points

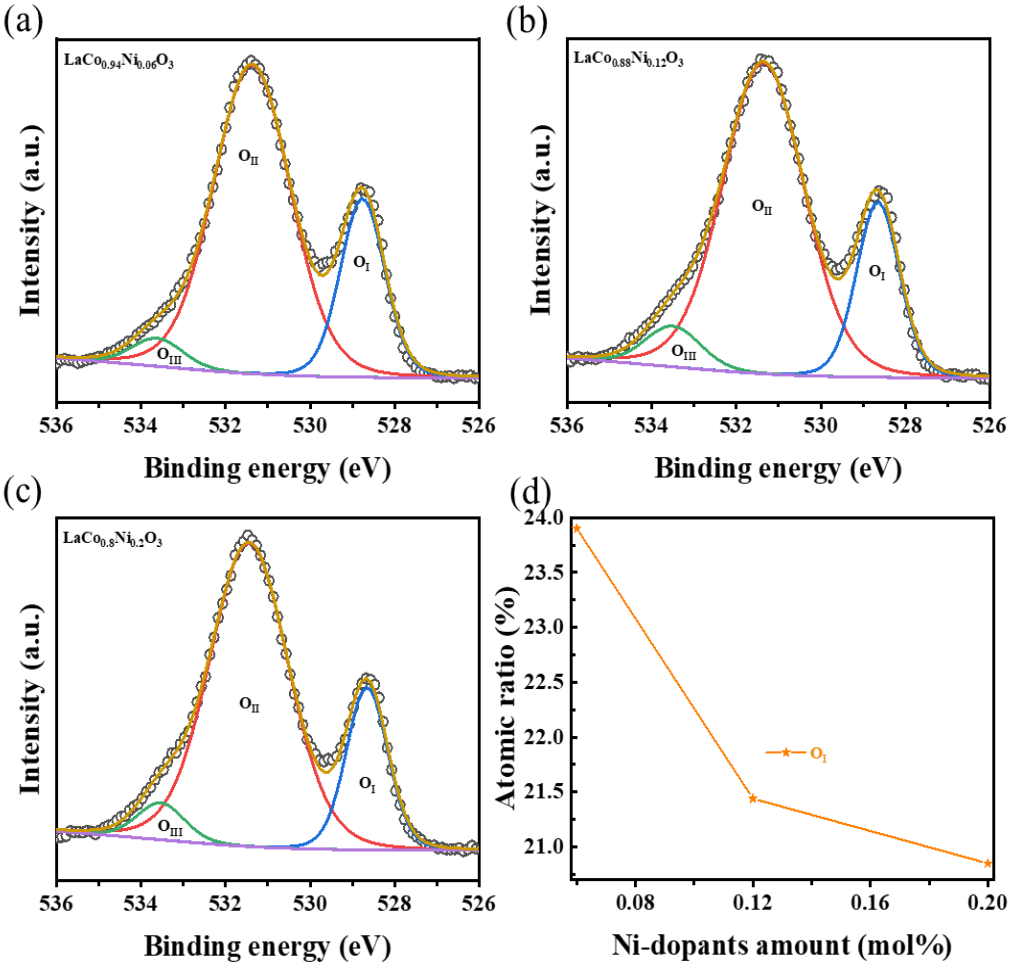

Fig. 4 High-resolution spectra of O 1s (a-c) and atomic ratio of O_I (d).

proves that the Drude model can be extended to lower frequencies. The resemble results have been demonstrated in composites with metal fillers distributed in an insulating matrix.[38-40] To evaluate the impact of Ni amounts on negative permittivity, the amplitude of negative permittivity is explored. The trend of absolute value of negative permittivity with Ni amounts is virtually identical to that of electrical conductivity. It is deduced that enhanced electrical conductivity can provide a giant negative permittivity. And this will be corroborated through analyzing the relationship negative permittivity and ac electrical conductivity.

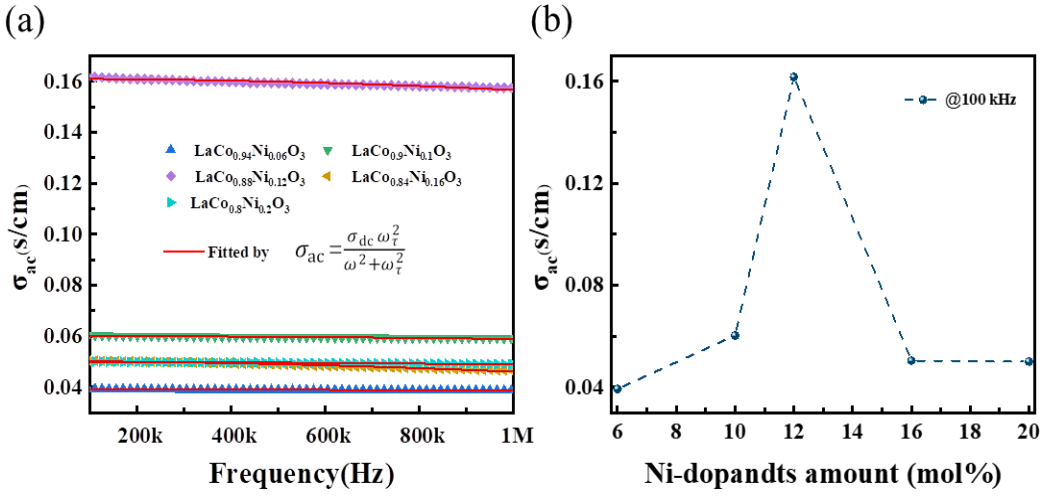

Fig. 5 Frequency-dependent (a) and Ni contents-dependent at 100 kHz (b) electrical conductivity.

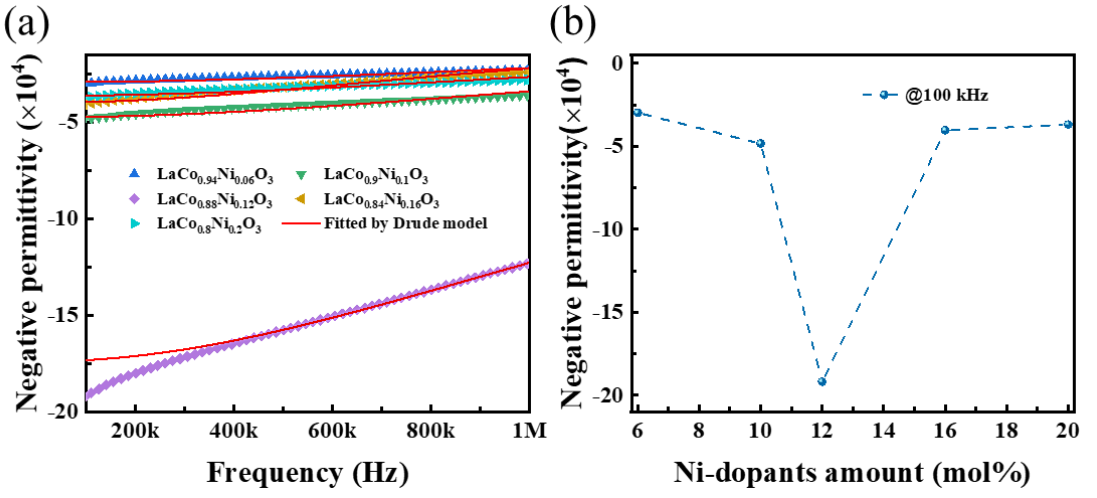

Fig. 6 Frequency-dependent (a) and Ni contents-dependent at 100 kHz (b) negative permittivity.

It is a generally accepted fact that permittivity properties of metals or metalloids are closely related to their electrical properties. Now, we elaborate their correlation in terms of electrodynamics. To find the effective parameters, one has to know the distribution of the electric field $\vec{E}(\omega)$ and current density $\vec{J}(\omega)$ in a system. And it's well established the relationship between current density and electrical field, complex conductivity $\sigma(\omega)$ is deduced below Eq. (3),

$$\sigma(\omega) = \frac{\sigma_0}{1-i\omega\tau}, \quad \sigma_0 = \frac{ne^2\tau}{m} \tag{3}$$

To obtain effective permittivity, we need bring $\vec{J}(\omega)$ into Maxwell equation, and we get the following equation $-\nabla^2\vec{E}(\omega) = \frac{\omega^2}{c^2}(1 + \frac{4\pi i\sigma(\omega)}{\omega})\vec{E}(\omega)$.

According to wave equation $-\nabla^2\vec{E}(\omega) = \frac{\omega^2}{c^2}\varepsilon(\omega)\vec{E}(\omega)$, the complex permittivity is deduced below Eq. (4),

$$\varepsilon(\omega) = 1 + \frac{4\pi i\sigma(\omega)}{\omega} \tag{4}$$

Substituting our earlier result for $\sigma(\omega)$, we find that

$$\varepsilon(\omega) = 1 - \frac{\frac{4\pi ne^2}{m}}{\omega^2 - i\omega\frac{1}{\tau}}, \tag{5}$$

Here we definite plasma frequency as $\omega_p^2 = \frac{4\pi ne^2}{m}$, damping parameter as $\gamma = \frac{1}{\tau}$,

and simply Eq. (5) as $\varepsilon(\omega) = 1 - \frac{\omega_p^2}{\omega^2 - i\omega\gamma}$.

From this, it is deduced that electrically Drude response of metalloid is necessary for realization of negative permittivity.

4. Conclusion

In this paper, we fabricated $LaCo_{1-x}Ni_xO_3$ ceramics and achieved plasma-like negative permittivity in kHz region. It is demonstrated the existence of low-frequency plasmonic state and extension of Drude model toward low frequencies. Furthermore, all designed specimens exhibited metalloid characteristics, but their electrical conductivities are limited in rise despite the increasing Ni contents. Similarly, amplitudes of negative permittivity show a dropping limit. It is proved that electrically Drude response of metalloid is necessary for realization of negative permittivity.

Acknowledgments

This work was supported by the National Natural Science Foundation of China (Nos. 51771104, 51871146, 51971119), the Natural Science Foundation of Shandong Province (No. ZR2020YQ32), and the Innovation Program of Shanghai Municipal Education Commission (No. 2019–01–07–00–10-E00053).

Conflict of Interest

There is no conflict of interest.

Supporting Information

Not applicable.

References

[1] P. Xie, W. Sun, A. Du, Q. Hou, G. Wu, R. Fan, Epsilon-negative carbon aerogels with state transition from dielectric to degenerate semiconductor, *Advanced Electronic Materials*, 2021, **7**, 2000877, doi: 10.1002/aelm.202000877.

[2] B. Li, G. Sui, W.H. Zhong, Single negative metamaterials in unstructured polymer nanocomposites toward selectable and

controllable negative permittivity, *Advanced Materials*, 2009, **21**, 4176-4180, doi: 10.1002/adma.200900653.

[3] C. H. Liu, N. Behdad, High-power microwave filters and frequency selective surfaces exploiting electromagnetic wave tunneling through ϵ-negative layers, *Journal of Applied Physics*, 2013, **113**, 064909, doi: 10.1063/1.4790584.

[4] Y. Li, N. Engheta, Capacitor-inspired metamaterial inductors, *Physical Review Applied*, 2018, **10**, 054021, doi: 10.1103/physrevapplied.10.054021.

[5] X. Song, G. Fan, D. Liu, Z. Wei, Y. Liu, R. Fan, Bilayer dielectric composites with positive-ε and negative-ε layers achieving high dielectric constant and low dielectric loss, *Composites Part A: Applied Science and Manufacturing*, 2022, **160**, 107071, doi: 10.1016/j.compositesa.2022.107071.

[6] D. Schurig, J. J. Mock, B. J. Justice, S. A. Cummer, J. B. Pendry, A. F. Starr, D. R. Smith, Metamaterial electromagnetic cloak at microwave frequencies, *Science*, 2006, **314**, 977-980, doi: 10.1126/science.1133628.

[7] J. B. Pendry, A. J. Holden, W. J. Stewart, I. Youngs, Extremely low frequency plasmons in metallic mesostructures, *Physical Review Letters*, 1996, **76**, 4773-4776, doi: 10.1103/physrevlett.76.4773.

[8] Z. Wei, Z. Wang, G. Fan, C. Xu, G. Shi, G. Zhang, Y. Liu, R. Fan, Low-frequency plasmonic state and negative permittivity in copper/titanium dioxide percolating composites, *Ceramics International*, 2021, **47**, 2208-2213, doi: 10.1016/j.ceramint.2020.09.060.

[9] Z. Wang, K. Sun, P. Xie, Q. Hou, Y. Liu, Q. Gu, R. Fan, Design and analysis of negative permittivity behaviors in Barium titanate/nickel metacomposites, *Acta Materialia*, 2020, **185**, 412-419, doi: 10.1016/j.actamat.2019.12.034.

[10] Z. Wang, K. Sun, P. Xie, Y. Liu, Q. Gu, R. Fan, Permittivity transition from positive to negative in acrylic polyurethane-aluminum composites, *Composites Science and Technology*, 2020, **188**, 107969, doi: 10.1016/j.compscitech.2019.107969.

[11] C. Cheng, Y. Liu, R. Ma, R. Fan, Nickel/yttrium iron garnet metacomposites with adjustable negative permittivity behavior toward electromagnetic shielding application, *Composites Part A: Applied Science and Manufacturing*, 2022, **155**, 106842, doi: 10.1016/j.compositesa.2022.106842.

[12] Y. Qu, Z. Wang, P. Xie, Z. Wang, R. Fan, Ultraweakly and fine-tunable negative permittivity of polyaniline/nickel metacomposites with high-frequency diamagnetic response, *Composites Science and Technology*, 2022, **217**, 109092, doi: 10.1016/j.compscitech.2021.109092.

[13] Z. Wang, K. Sun, P. Xie, R. Fan, Y. Liu, Q. Gu, J. Wang, Low-loss and temperature-stable negative permittivity in La0.5Sr0.5MnO3 ceramics, *Journal of the European Ceramic Society*, 2020, **40**, 1917-1921, doi: 10.1016/j.jeurceramsoc.2020.01.024.

[14] G. Fan, Z. Wang, H. Ren, Y. Liu, R. Fan, Dielectric dispersion of copper/rutile cermets: Dielectric resonance, relaxation, and plasma oscillation, *Scripta Materialia*, 2021, **190**, 1-6, doi: 10.1016/j.scriptamat.2020.08.027.

[15] H. Wu, X. Huang, L. Qian, Recent Progress on the Metacomposites with Carbonaceous Fillers, *Engineered Science*, 2018, **2**, 17-25, doi: 10.30919/es8d656.

[16] T. Tsutaoka, H. Massango, T. Kasagi, S. Yamamoto, K. Hatakeyama, Double negative electromagnetic properties of percolated Fe53Ni47/Cu granular composites, *Applied Physics Letters*, 2016, **108**, 191904, doi: 10.1063/1.4949560.

[17] H. Gu, J. Guo, Q. He, Y. Jiang, Y. Huang, N. Haldolaarachige, Z. Luo, D. P. Young, S. Wei, Z. Guo, Magnetoresistive polyaniline/multi-walled carbon nanotube nanocomposites with negative permittivity, *Nanoscale*, 2014, **6**, 181-189, doi: 10.1039/c3nr04152b.

[18] X. Yao, X. Kou, J. Qiu, Multi-walled carbon nanotubes/polyaniline composites with negative permittivity and negative permeability, *Carbon*, 2016, **107**, 261-267, doi: 10.1016/j.carbon.2016.05.055.

[19] H. Gu, X. Xu, M. Dong, P. Xie, Q. Shao, R. Fan, C. Liu, S. Wu, R. Wei, Z. Guo, Carbon nanospheres induced high negative permittivity in nanosilver-polydopamine metacomposites, *Carbon*, 2019, **147**, 550-558, doi: 10.1016/j.carbon.2019.03.028.

[20] P. Xie, Z. Shi, M. Feng, K. Sun, Y. Liu, K. Yan, C. Liu, T. A. A. Moussa, M. Huang, S. Meng, G. Liang, H. Hou, R. Fan, Z. Guo, Recent advances in radio-frequency negative dielectric metamaterials by designing heterogeneous composites, *Advanced Composites and Hybrid Materials*, 2022, **5**, 679-695, doi: 10.1007/s42114-022-00479-2.

[21] K. Sun, J. Dong, Z. Wang, Z. Wang, G. Fan, Q. Hou, L. An, M. Dong, R. Fan, Z. Guo, Tunable negative permittivity in flexible graphene/PDMS metacomposites, *The Journal of Physical Chemistry C*, 2019, **123**, 23635-23642, doi: 10.1021/acs.jpcc.9b06753.

[22] G. Fan, Z. Wang, K. Sun, Y. Liu, R. Fan, Doped ceramics of indium oxides for negative permittivity materials in MHz-kHz frequency regions, *Journal of Materials Science & Technology*, 2021, **61**, 125-131, doi: 10.1016/j.jmst.2020.06.013.

[23] G. Fan, Z. Wang, K. Sun, Y. Liu, R. Fan, Doping-dependent negative dielectric permittivity realized in mono-phase antimony tin oxide ceramics, *Journal of Materials Chemistry C*, 2020, **8**, 11610-11617, doi: 10.1039/d0tc02266g.

[24] G. Nirala, D. Yadav, T. Katheriya, S. Upadhyay, Temperature dependent negative permittivity in solid solutions $Sr_2Mn_{1-x}Sn_xO_4$ (x = 0, 0.3, 0.5), *Journal of the European Ceramic Society*, 2022, **42**, 453-461, doi: 10.1016/j.jeurceramsoc.2021.10.056.

[25] K.-L. Yan, R.-H. Fan, Z.-C. Shi, M. Chen, L. Qian, Y.-L. Wei,

K. Sun, J. Li, Negative permittivity behavior and magnetic performance of perovskite La1–xSrxMnO$_3$ at high-frequency, *Journal of Materials Chemistry C*, 2014, **2**, 1028-1033, doi: 10.1039/c3tc31906g.

[26] F. Wang, W. Gu, J. Chen, Y. Wu, M. Zhou, S. Tang, X. Cao, P. Zhang, G. Ji, Improved electromagnetic dissipation of Fe doping LaCoO3 toward broadband microwave absorption, *Journal of Materials Science & Technology*, 2022, **105**, 92-100, doi: 10.1016/j.jmst.2021.06.058.

[27] F. Wang, W. Gu, J. Chen, Y. Wu, M. Zhou, S. Tang, X. Cao, P. Zhang, G. Ji, The point defect and electronic structure of K doped LaCo0.9Fe0.1O3 perovskite with enhanced microwave absorbing ability, *Nano Research*, 2022, **15**, 3720-3728, doi: 10.1007/s12274-021-3955-1.

[28] Z. Wei, Z. Wang, C. Xu, G. Fan, X. Song, Y. Liu, R. Fan, Defect-induced insulator-metal transition and negative permittivity in La1-Ba CoO3 perovskite structure, *Journal of Materials Science & Technology*, 2022, **112**, 77-84, doi: 10.1016/j.jmst.2021.11.002.

[29] O. Ryotaro, Simple model for estimating band edge wavelengths of selective reflection from cholesteric liquid crystals for oblique incidence, *Physical Review E*, 2019, **100**, 012708, doi: 10.1103/PhysRevE.100.012708.

[30] A. A. Ansari, S. F. Adil, M. Alam, N. Ahmad, M. E. Assal, J. P. Labis, A. Alwarthan, Catalytic performance of the Ce-doped LaCoO$_3$ perovskite nanoparticles, *Scientific Reports*, 2020, **10**, 15012, doi: 10.1038/s41598-020-71869-z.

[31] P. Liang, D. Meng, Y. Liang, Z. Wang, C. Zhang, S. Wang, Z. Zhang, Cation deficiency tuned LaCoO$_{3-\delta}$ perovskite for peroxymonosulfate activation towards bisphenol A degradation, *Chemical Engineering Journal*, 2021, **409**, 128196, doi: 10.1016/j.cej.2020.128196.

[32] M. S. Khalil, Synthesis, X-ray, infrared spectra and electrical conductivity of La/Ba–CoO$_3$ systems, *Materials Science and Engineering: A*, 2003, **352**, 64-70, doi: 10.1016/S0921-5093(02)00557-9.

[33] Z. Wang, X. Li, L. Wang, Y. Li, J. Qin, P. Xie, Y. Qu, K. Sun, R. Fan, Flexible multi-walled carbon nanotubes/polydimethylsiloxane membranous composites toward high-permittivity performance, *Advanced Composites and Hybrid Materials*, 2020, **3**, 1-7, doi: 10.1007/s42114-020-00144-6.

[34] Z. Wang, K. Sun, Y. Qu, Z. Wang, J. Tian, X. Li, R. Fan, Negative-k and positive-k layers introduced into graphene/polyvinylidene fluoride composites to achieve high-k and low loss, *Materials & Design*, 2021, **209**, 110009, doi: 10.1016/j.matdes.2021.110009.

[35] M. Ali Bousnina, F. Giovannelli, L. Perriere, G. Guegan, F. Delorme, Ba substitution for enhancement of the thermoelectric properties of LaCoO3 ceramics (0⩽x⩽0.75), Journal of Advanced Ceramics, 2019, **8**, 519-526, doi: 10.1007/s40145-019-0333-5.

[36] K. Sun, W. Duan, Y. Lei, Z. Wang, J. Tian, P. Yang, Q. He, M. Chen, H. Wu, Z. Zhang, R. Fan, Flexible multi-walled carbon nanotubes/polyvinylidene fluoride membranous composites with weakly negative permittivity and low frequency dispersion, *Composites Part A: Applied Science and Manufacturing*, 2022, **156**, 106854, doi: 10.1016/j.compositesa.2022.106854.

[37] J. Tian, R. Fan, Z. Zhang, Y. Li, H. Wu, P. Yang, P. Xie, W. Duan, C.-S. Lee, Flexible and biocompatible poly (vinyl alcohol)/multi-walled carbon nanotubes hydrogels with epsilon-near-zero properties, *Journal of Materials Science & Technology*, 2022, **131**, 91-99, doi: 10.1016/j.jmst.2022.05.019.

[38] Z. Zhang, M. Liu, M. M. Ibrahim, H. Wu, Y. Wu, Y. Li, G. A. M. Mersal, I. H. El Azab, S. M. El-Bahy, M. Huang, Y. Jiang, G. Liang, P. Xie, C. Liu, Flexible polystyrene/graphene composites with epsilon-near-zero properties, *Advanced Composites and Hybrid Materials*, 2022, **5**, 1054-1066, doi: 10.1007/s42114-022-00486-3.

[39] M. Liu, H. Wu, Y. Wu, P. Xie, R. A. Pashameah, H. M. Abo-Dief, S. M. El-Bahy, Y. Wei, G. Li, W. Li, G. Liang, C. Liu, K. Sun, R. Fan, The weakly negative permittivity with low-frequency-dispersion behavior in percolative carbon nanotubes/epoxy nanocomposites at radio-frequency range, *Advanced Composites and Hybrid Materials*, 2022, **5**, 2021-2030, doi: 10.1007/s42114-022-00541-z.

[40] G. Fan, T. Feng, Y. Qu, C. Hao, Y. Liu, Dielectric properties and negative permittivity performance modulated by dual fillers in CNTs/TiN/CaCu$_3$Ti$_4$O$_{12}$ ternary composites, *Ceramics International*, 2022, **48**, 28135-28141, doi: 10.1016/j.ceramint.2022.06.118.

